

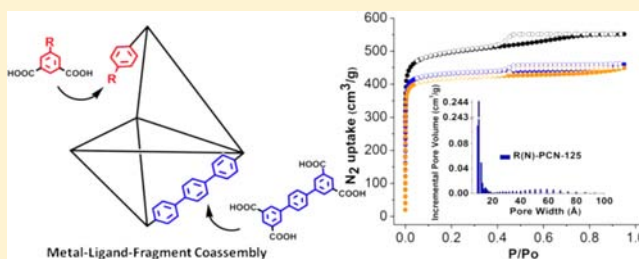
Introduction of Functionalized Mesopores to Metal–Organic Frameworks via Metal–Ligand–Fragment Coassembly

Jinhee Park, Zhiyong U. Wang, Lin-Bing Sun, Ying-Pin Chen, and Hong-Cai Zhou*

Department of Chemistry, Texas A&M University, P.O. Box 30012, College Station, Texas 77842-3012, United States

S Supporting Information

ABSTRACT: Introduction of functionalized mesopores into microporous metal–organic frameworks (MOFs) can endow them with suitable properties for applications in gas storage, separation, catalysis, and drug delivery. However, common methods for functionalization (including pre- and post-synthetic modifications) of the internal surface of a MOF reduce the pore size of the MOF because the additional functional groups fill up the pores. We present a metal–ligand–fragment coassembly strategy for the introduction of (meso)pores functionalized with various substituent groups on the ligand fragments. Astonishingly, this new functionalization strategy *increases* the pore volume of a MOF instead of reducing it. Since the ligand fragments are often readily available or easily prepared, the new procedure for synthesis of the modified MOFs becomes much easier and more applicable than existing approaches. Remarkably, mesopores can be generated conveniently and controllably by the coassembly of a ligand and its fragment containing the desired functional groups. The fragment/ligand ratio has been optimized to preserve the parent structure and to promote maximum mesopore introduction, which has led to a systematic evaluation of the effectiveness of a series of functional groups for the adsorption of guest molecules.



INTRODUCTION

Metal–organic frameworks (MOFs) are porous crystalline materials assembled through coordination between two types of building units: metal or metal-containing nodes and organic linkers. The structure, pore size, and surface functionalities of MOFs can be tailored by judicious choices of these building blocks,¹ thus leading to diverse applications of MOFs such as in selective gas separation,² gas storage,³ chemical sensing,⁴ biomedical applications,⁵ and catalysis.⁶ Generally, the functionalization of MOF interiors has relied on the pre-installation of ligands with desired functional groups or post-modification of ligands bearing reactive groups such as alkynes or amines.⁷ Despite their success, both pre-functionalization and post-modification generally suffer from the same limitation, namely, that the pore size of the functionalized MOF is reduced compared to that of the parent MOF because the additional functional groups point toward the pores, thus occupying free volume. This often results in reduction of both the surface area and uptake of guest molecules, which is undesirable for practical applications. Herein, we report a versatile strategy to introduce not only functional groups but also functionalized cavities into microporous MOFs through one-fell-swoop assembly of a primitive ligand and its fragments. As discussed below in detail, our functionalization approach leads to the formation of mesopores decorated with various functional groups in originally microporous MOFs. Our approach bears some resemblance to the well-established mixed-ligand approach. For the latter, surface functionalization can be achieved by the coassembly of the same topological ligands

containing different substituent groups. For example, complex MOFs with linear bridging ligands such as terephthalate and its derivatives have been reported by the Yaghi group^{7b} and the Matzger group.⁸ However, since it is difficult to synthesize complex ligands with various substituent groups, this functionalization method cannot be generally used in diverse structural MOFs. Another approach uses coordination copolymerization of structurally distinct ligands, such as extended ligands and small simple ones to build mixed-ligand MOFs, introduced in part by the Matzger group.⁹ The resulting MOFs are generally not isostructural to the parent MOF, making it hard to predict the outcome of the functionalization. In contrast, in metal–ligand–fragment coassembly, the two ligands, the primitive ligand and its fragment, are crystallized into MOFs that are isostructural to the parent MOF derived from only the primitive ligand.

Coassembly of the ligand and its fragment into one MOF can bring new opportunities. The interior of the MOFs can be tuned by a wide variety of functional groups on the ligand fragments, including polar and ionic ones, while maintaining the structure of the parent MOF. Most of the ligand fragments in this report are readily available or relatively easily prepared. Thus the synthesis of the functionalized MOFs becomes easier and more applicable than previously reported functionalization methods. In addition, the functionalized MOFs maintain the isostructure of the unfunctionalized ones, thus allowing a

Received: August 29, 2012

Published: November 19, 2012

systematic study on the functional groups. Interestingly, depending on the functional groups on the ligand fragments, the introduced cavities can be extended to mesopores in a convenient and controllable manner.¹⁰ Such mixed micro- and mesopores in one MOF are suitable for both high guest uptake and efficient mass transport into and out of the pores, resulting in their technological applications in catalysis, separation, and fuel gas storage, among others.¹¹

Porous polymers have been prepared by a similar method. Tetrahedral and truncated trigonal monomers are co-condensed to form three-dimensional networks. The truncated monomers have functional groups such as catalytic sites or long alkyl chains on the truncated site.¹² Therefore, the pores of the polymers contain the functionalities originated from the truncated monomers. This is the first time a ligand fragmentation strategy has been used in crystalline MOFs, enabling preparation of isostructure but functionally versatile mesoporous MOFs.

RESULT AND DISCUSSION

We initiated a metal–ligand–fragment coassembly strategy in which a NbO-type topological MOF (NOTT-101) with terphenyltetracarboxylates (TPTCs) and dicopper paddlewheel SBUs (secondary building units) was chosen as a model structure due to its robustness and high CO₂ and H₂ uptake capacity for clean energy-related applications.¹³ 5-R isophthalate (R-isoph, where R represents functional groups such as methyl, amino, aminomethyl, nitro, sulfo, and sodium sulfo groups) can be considered as a functionalized fragment of TPTC because it is in the form of a truncated TPTC by replacing one half of TPTC, namely biphenyl dicarboxylate, with R substituents (Figure 1). In R-isoph, its carboxylate

moieties will coordinate to Cu²⁺ by forming Cu paddlewheel clusters, and the R group will modify the MOF interior. Because R-isoph is shorter than TPTC, its introduction into the frameworks will result in the formation of large pores. For our approach to be effective, the MOF structure should be stable enough to bear the ligand fragments that lead to incomplete connectivity between the ligands and metal nodes. Furthermore, the primitive ligand and its fragments should have comparable reactivity toward metal ions. Otherwise, the fragments would be excluded from the crystal structure. Previously, in a coordination modulation method reported by the Kitagawa group, a capping additive, monocarboxylate, was employed in MOF synthesis. The additive mainly influenced the morphology and size of the MOFs via competitive interaction with a linker, leading to hierarchical micro- and mesoporous structures with mesoporous grain boundaries.¹⁴ The same group reported a method for the modular design of mesoscale domain assembly in porous coordination polymers based on the kinetic difference between the precursors in crystal formation.¹⁵ In our method, because R-isoph and TPTC have the same basic coordination moiety, they become difficult to discriminate during the crystal formation and are distributed throughout the crystals, providing functionalized cavities in the MOFs. This kind of heterogeneity, originating from the additional ligands (here R-isoph), has rarely been reported because crystallization is a slow and reversible process capable of repairing nonperiodic inclusion.¹⁶

We are excited to report that the metal–ligand–fragment coassembly strategy indeed works. Under solvothermal conditions, the primitive ligand (TPTC) and its fragment (R-isoph) are randomly inserted into the crystal lattice while the original crystal structure is maintained. Newly assembled MOFs with TPTC and R-isoph are designated as R(*N*)-PCN-125. PCN represents porous coordination network, and the parenthesized *N* indicates the molar ratio of R-isoph to H₄TPTC in the feed. Generally, R(*N*)-PCN-125 was prepared by adding Cu(NO₃)₂·6H₂O into an *N,N*-dimethylacetamide solution of H₄TPTC and H₂R-isoph mixtures. Synthesized R(*N*)-PCN-125 was characterized by powder X-ray diffraction (PXRD) and N₂ gas adsorption measurements to study its crystallinity, its permanent porosity, and the formation of micro- and mesopores. Although we have determined the crystal structure of R(*N*)-PCN-125 via single-crystal X-ray diffraction, we were unable to visualize the accommodation state of the primitive ligand and its fragment, presumably due to their random distribution over the crystals.

First, incorporation of the simplest ligand fragment, isophthalate (H-isoph), was examined to test the feasibility of our approach. The crystals were formed in the isostructure with feed ratios of H₄TPTC and H₂H-isoph from 4:1 to 1:8 as confirmed by the PXRD patterns of the crystalline powders (H-PCN-125), in good agreement with LeBail fittings (Figures 2a and S5).¹³ Although the feed ratio 1:8 of H₄TPTC to H₂H-isoph still yielded crystalline H-PCN-125, broadening of the PXRD peaks indicated decreased framework crystallinity.¹⁷ The full width at half intensity of the (2 -1 0) reflection (at 2θ ≈ 9.4°) of H-PCN-125 increased from 0.14° to 0.18° when the feed ratio increased from 1:0.25–2 to 1:4–8 (Figure S4). In addition, the crystals prepared from the feed ratio of 1:4 of H₄TPTC to H₂R-isoph showed dramatically diminished clarity compared with the crystals prepared from the low feed ratio (Figure 3b,c). Accordingly, we determined that feed ratios 1:1 or 1:2 of H₄TPTC to H₂R-isoph were optimal to synthesize

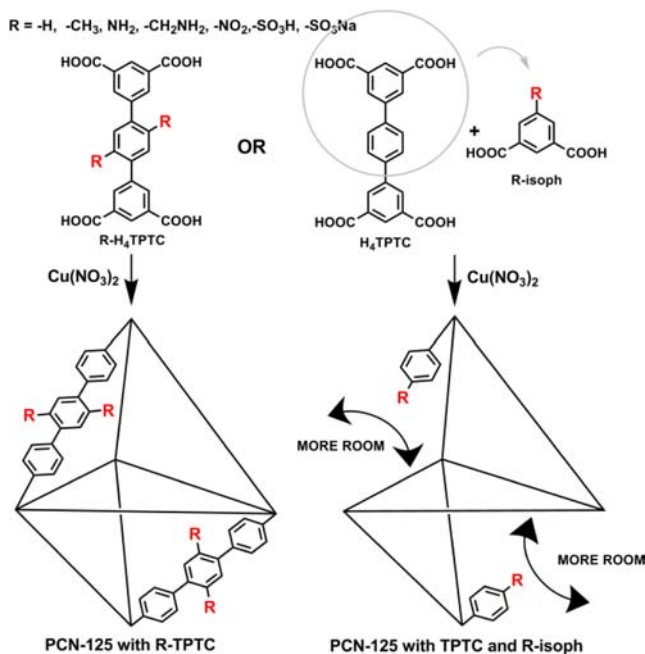


Figure 1. Schematic illustration of the ligand truncation method. When R-H₄TPTC reacts with Cu(NO₃)₂, the MOF has R groups pointing into pores (left), which might reduce the pore size. On the other hand, copolymerization of TPTC and R-isoph gives the MOF having increased pore size due to the truncated ligands (right). Scaffold represents one of the pores of PCN-125 with R-TPTC (left) and with TPTC and R-isoph (right).

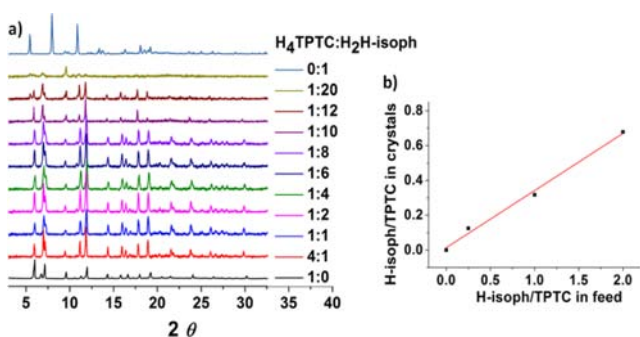


Figure 2. (a) PXRD data for H(N)-PCN-125 prepared from various feed ratios of H₄TPTC and H₂H-isoph (1:0, 4:1, 1:1, 1:2, 1:4, 1:6, 1:8, 1:10, 1:12, 1:20, and 0:1). (b) Plot of H-isoph/TPTC in crystals vs H-isoph/TPTC in feed.

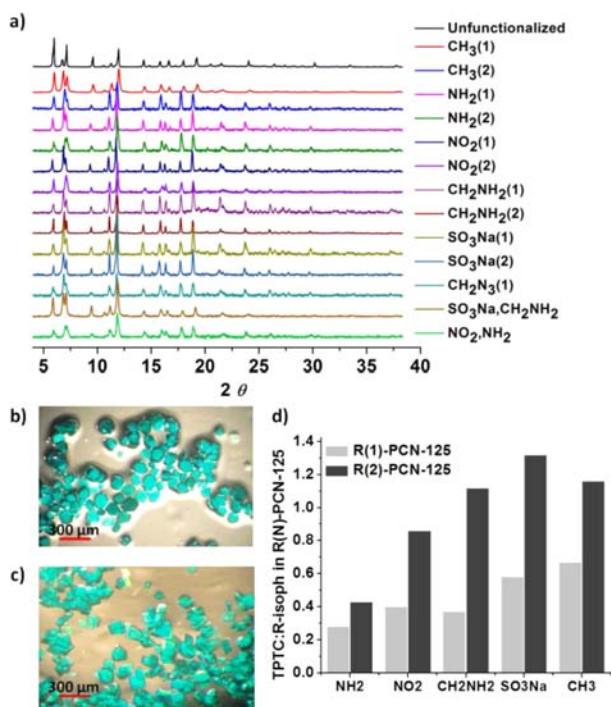


Figure 3. (a) PXRD patterns showing that all R(N)-PCN-125 presented in this report are isostructural. In the legend, the formulas indicate the functional group (R) and the feed ratio (N) in R(N)-PCN-125. (b) Photograph of NO₂(2)-PCN-125 crystals. (c) Photograph of H(4)-PCN-125 crystals. (d) Incorporation ratios analyzed by NMR after digesting R(1 or 2)-PCN-125.

functionalized MOFs via metal–ligand–fragment coassembly. It is important to mention that pure H-isoph can crystallize in a totally different phase under identical conditions (Figure 2a). Thus, if H-isoph is not incorporated in the parent structure, the peaks from a crystal solely with H-isoph and Cu²⁺ should appear in a mixed PXRD pattern.¹⁵ When the feed ratio became 1:10, an additional reflection (at $2\theta = 5.47$) appeared, resulting from the crystal derived solely from H-isoph. It means that the maximum feed ratio is 1:8. Despite the unchanging PXRD results, the inclusion of H-isoph in H-PCN-125 was revealed by NMR analysis after the MOF crystals were digested in DCl/DMSO-*d*₆. The quantity of H-isoph in H-PCN-125 was determined by comparing integration of the resonance at 7.84 ppm, corresponding to the four protons in the middle benzene group of TPTC, with the one at 7.67 ppm,

corresponding to a proton on the fifth carbon of H-isoph. Since H-isoph amounts in H-PCN-125 were linearly correlated with the ones in feed, the degree of functionalization can be controlled by the feed ratio of H₄TPTC to H₂H-isoph (Figure 2b). Based on PXRD patterns which confirm phase purity and NMR results containing the peaks from both TPTC and H-isoph, the possibility of the formation of two different MOFs with each of TPTC and H-isoph was ruled out.

The successful incorporation of H-isoph into the MOFs without disturbing the overall MOF structure prompted us to try other R-isoph with useful functional groups at the 5-position such as methyl, amine, methylamine, nitro, sulfo, and sodium sulfo groups. These R-functionalized MOFs crystallized in the same crystal system, as evidenced by PXRD measurements (Figure 3a). As shown in the photograph of NO₂(2)-PCN-125, the crystallinity of the MOFs can be well-maintained even with the incorporation of NO₂-isoph (Figure 3b). Each R-isoph shows different incorporation ratios, as shown in Figure 3d. When the feed ratio of H₄H-TPTC to H₂isoph was changed from 1:1 to 1:2, the incorporated amount was also increased while the incorporation trend of each R-isoph was nearly preserved. This demonstrates that the amount of the functional groups in the frameworks can be tuned by changing the feed ratios. Thermogravimetric analysis (TGA) showed high thermal stability of R(N)-PCN-125 up to 300 °C, comparable to that of unfunctionalized PCN-125. SO₃Na(1)-PCN-125 has the highest degradation temperature (320 °C) among all R(N)-PCN-125 (Figure S13).

N₂ adsorption isotherms at 77 K for three samples of H-PCN-125 prepared in different molar ratios of H₄TPTC to H₂H-isoph (4:1, 1:1, and 1:2) were measured to determine their permanent porosity, architectural rigidity, and pore size distribution. The 4:1 feed ratio resulted in almost the same N₂ uptake as that of unfunctionalized PCN-125. When the H₄TPTC/H₂H-isoph ratio was increased to 1:2, H-PCN-125 still retained high surface areas (2200–1650 m² g⁻¹) while maintaining a type I N₂ adsorption isotherm with a 28% decrease in total uptake capacity. More importantly, the pore widths gradually increased, as shown in Figure 4a. Since R-isoph is shorter than TPTC, the decreased surface area and increased pore width demonstrate the well-dispersed R-isoph throughout the frameworks. CH₃(1 and 2)- and NH₂(1 and 2)-PCN-125 showed a similar trend of decreased N₂ uptake and the step-by-step broadening of the pore size distribution (Figure 4b). In most traditional surface functionalization methods, functional groups dangle into pores and result in decreased pore size. In contrast, the functional groups in this metal–ligand–fragment coassembly are pointing toward the pores generated via the incorporation of R-isoph, leading to increased pore size with the desired functionalities (Figure 1). The Brunauer–Emmett–Teller (BET) and Langmuir surface areas and pore volumes of all R(N)-PCN-125 prepared in different feed ratios are presented in Table S5.

The step-by-step broadening of the pore size distributions in H- and NH₂-PCN-125 indicates that these R-isoph and TPTC are evenly dispersed throughout the crystal structure. Based on this finding, we hypothesized that if the interaction between individual R-isophs or between individual TPTCs is bigger than the interaction between R-isoph and TPTC, R-isoph and TPTC cannot be thoroughly mixed and well-dispersed over the crystal lattice, leading to the formation of domains containing more fragment ligands. Because the fragment ligands are smaller and have fewer coordination groups than the primitive

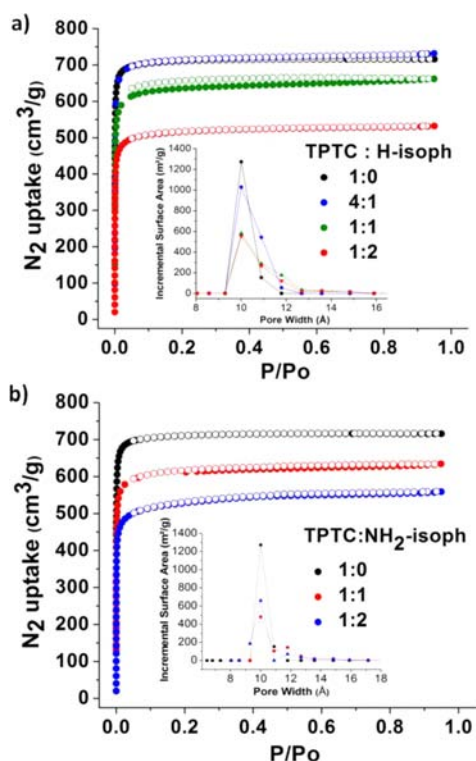


Figure 4. N_2 adsorption isotherms of unfunctionalized PCN-125 and H(0.25, 1, and 2)-PCN-125 (a) and unfunctionalized PCN-125 and NH_2 (1 and 2)-PCN-125 (b). Each legend indicates the feed ratios of H_4 TPTC and R-isoph. Insets show the pore size distribution of H- (a) and NH_2 -PCN-125 (b).

ligand, they play a role in breaking a wall (formed by TPTC in unfunctionalized PCN-125) between neighboring pores and combining the pores to give larger pores. In this domain, more pores are combined into one pore, generating bigger cavities (mesopores) in the MOFs. Along this line, the R-isoph, having polar, ionic, or bigger functional groups, is introduced to increase the interaction between individual R-isophs or between individual TPTCs. Generally, these functional groups on the organic linkers occupy more space in the pore, leading to a significant decrease of pore size in the MOFs. In contrast, the MOFs functionalized via metal–ligand–fragment coassembly show that the introduced cavities can be increased up to the mesoporous region. CH_2NH_2 -, SO_3H -, SO_3Na -, and NO_2 -PCN-125 were found to have type IV N_2 adsorption isotherms (characteristic of mesoporous materials), in contrast to unfunctionalized PCN-125.¹⁴ Although we used the primary amine form of CH_2NH_2 -isoph in the feed, it became ionic in CH_2NH_2 -PCN-125 during the solvothermal synthesis, as revealed by CO_2 adsorption. CO_2 adsorption of CH_2NH_2 -PCN-125 did not show a significant uptake increase in the low pressure range, which is usually observed in porous materials containing primary amines.¹⁸ Each R(N)-PCN-125 requires an optimized feed ratio to form mesopores, and further increasing or decreasing the amount of R-isoph diminished the hysteresis loop noticeably (see Supporting Information section S-5-b). Through the optimization process, we found that CH_2NH_2 (1)-, SO_3H (1)-, SO_3Na (2)-, and NO_2 (2)-PCN-125 showed combined isotherms of types I and IV (Figure 5a). That is, the isotherms have a steep rise in the low pressure range and pronounced hysteresis in the desorption branch. The results indicate that the pores of those MOFs are hierarchically

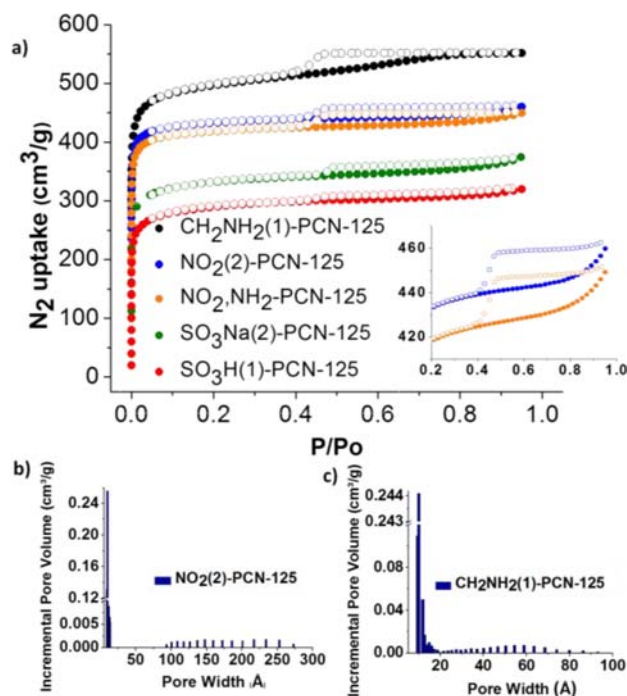


Figure 5. (a) N_2 adsorption isotherms of mesoporous R(N)-PCN-125: CH_2NH_2 (1)-, NO_2 (2)-, NO_2,NH_2 -, SO_3Na (2)-, and SO_3H (1)-PCN-125. Inset shows the hysteresis generated from the mesoporosity in NO_2 (2)-PCN-125 and NO_2,NH_2 -PCN-125. (b) Pore size distribution of NO_2 (2)-PCN-125 calculated by the DFT method. (c) Pore size distribution of CH_2NH_2 (1)-PCN-125 calculated by the DFT method.

constructed from both mesopores and micropores. For example, NO_2 (2)-PCN-125 possesses mesopores with 200 Å diameter and micropores with 10 Å diameter, as determined by a density functional theory (DFT)-based method (Figure 5b). CH_2NH_2 (1)-PCN-125 has mesopores with a diameter of 58 Å and micropores with a diameter of 10 Å, as determined by the DFT-based method (Figure 5c). While micropore distributions are mainly centered at a diameter 10 Å, the distributions of the introduced mesopores vary depending on R-isoph. In addition, ratios of micro- to mesopores are calculated on the basis of the pore size distribution (Table S4). The ratios range from 5.5 (CH_2NH_2 (1)-PCN-125) to 19.5 (NO_2 (2)-PCN-125), demonstrating the modulation of the size and ratio of generated mesopores in microporous MOFs via changing fragment ligands and their feed ratios during solvothermal synthesis.

As a further extension of this strategy, not only single but also multiple functional groups were immobilized in R,R'-PCN-125 by the use of two different R- and R'-isoph fragments in the feed. For example, NO_2,NH_2 -PCN-125 was prepared by mixing two different truncated ligands in a 1:1:2 feed ratio (H_2NO_2 -isoph: H_2NH_2 -isoph: H_4 TPTC) and characterized by PXRD, NMR, and N_2 adsorption measurements. The N_2 adsorption isotherm of NO_2,NH_2 -PCN-125 shows a noticeable hysteresis loop, indicating mesoporosity of the MOF, while its NMR spectrum has resonances from two truncated ligands, NO_2 -isoph and NH_2 -isoph (Figures 4a and S5). Although NH_2 (1 and 2)-PCN-125 and NO_2 (1)-PCN-125 did not show mesoporosity, combination of NO_2 -isoph and NH_2 -isoph can generate amine- and nitro-functionalized mesopores in the MOFs. This implies that our metal–ligand–fragment coassembly approach can be used in the preparation of multifunc-

tional MOFs. For instance, in the catalysis application of NO_2/NH_2 -PCN-125, NH_2 -isoph can provide base catalytic active sites while NO_2 -isoph grants spacious room for efficient substrate and product transport into and out of NO_2/NH_2 -PCN-125. Such synergy is the key for practical application of MOFs in catalysis.

Another salient feature of $R(N)$ -PCN-125 is the enhanced interaction with guest molecules due to the introduced functionalities. As an experimental proof-of-concept, CO_2 adsorption in the low pressure range, accompanied with high heat of CO_2 adsorption, was demonstrated. All the heats of adsorption were calculated by fitting a virial-type equation to both 273 K and room-temperature CO_2 adsorption isotherms.¹⁹ Although $\text{NH}_2(1)$ -, $\text{CH}_3(1)$ -, and $\text{NO}_2(1)$ -PCN-125 possessed lower surface areas, their CO_2 uptake at 273 K and heats of adsorption were either higher or similar compared with those of their unfunctionalized counterparts (Figure 6a).

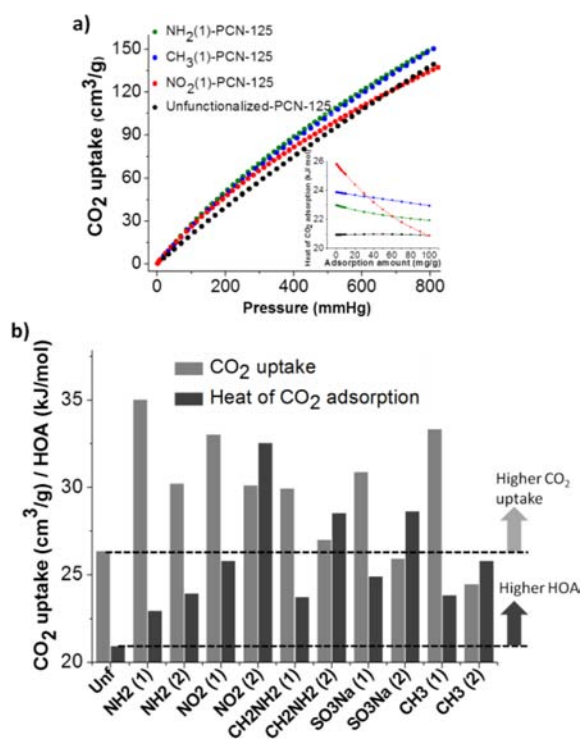


Figure 6. (a) CO_2 adsorption isotherms for $\text{NH}_2(1)$ -, $\text{CH}_3(1)$ -, and $\text{NO}_2(1)$ -PCN-125 and unfunctionalized PCN-125, represented by green, blue, red, and black, respectively. Inset shows the loading dependence of the isosteric heats of CO_2 adsorption in $R(N)$ -PCN-125. (b) Light gray bars show the CO_2 uptake of $R(N)$ -PCN-125 at 273 K and 130 mmHg. Heats of CO_2 adsorption of each $R(N)$ -PCN-125 are calculated on the basis of CO_2 adsorption isotherms at 273 K and room temperature (dark gray bars). All of the CO_2 adsorption isotherms and loading dependence of the isosteric heats of CO_2 adsorption can be found in Supporting Information section 6.

In order to exclude the temperature variation between the measurements and examine interaction strength between CO_2 and the frameworks, CO_2 uptake results for $R(N)$ -PCN-125 at 273 K and 130 mmHg instead of at room temperature and 1 atm were analyzed and compared with the performance of unfunctionalized PCN-125 (Figures 6b and S6). CO_2 uptake capacities in most of $R(N)$ -PCN-125 were higher than those of unfunctionalized PCN-125, and all R -isoph showed improved heats of CO_2 adsorption. For example, $\text{NH}_2(1)$ -PCN-125

shows 30% higher CO_2 uptake at 130 mmHg than unfunctionalized PCN-125, and $\text{NO}_2(2)$ -PCN-125 has the highest heat of CO_2 adsorption: 32.5 kJ/mol (50% increase). Interestingly, H - and CH_3 -PCN-125 also showed increased heats of CO_2 adsorption. This can be reasoned as follows: because of the lack of high connectivity between the ligands and metal nodes in $R(N)$ -PCN-125, uncoordinated carboxylate groups of TPTC or metal clusters might serve as additional favorable CO_2 adsorption sites. Hence, the results indicate that most $R(N)$ -PCN-125 are better adsorbents for CO_2 capture than the unfunctionalized PCN-125.

CONCLUSIONS

In summary, the metal–ligand–fragment coassembly strategy was studied to introduce functionalized mesopores in MOFs. The primitive ligand (TPTC) and its ligand fragment (R -isoph) were coassembled to generate a series of the isostructural MOFs with pendant functional groups (R). Importantly, depending on the functional groups, mesopores were generated in the microporous structure, confirmed by N_2 adsorption isotherms. The degree of mesoporosity could be controlled by changing R -isoph and the feed ratios of H_4TPTC and R -isoph. The hierarchical micro- and mesopores in MOFs can improve the mass transport, leading the utilization of the MOFs in applications such as catalysis, separation, and gas storage. Since most of the truncated ligands used here were easily prepared, the ligand fragmentation method becomes more practical when compared with traditional surface modification methodology. In addition, the multifunctional surface may become useful in multistep catalytic reactions²⁰ and multipurpose sensor fabrication.²¹ Based on the findings in this report, we are exploring the generality of this approach to other types of frameworks and its practical applications such as in selective gas adsorption and cooperative catalysis.

EXPERIMENTAL SECTION

Instruments. ^1H nuclear magnetic resonance (NMR) data to confirm the ligand synthesis and incorporation of R -isoph and TPTC in each $R(N)$ -PCN-125 were recorded on a Mercury 300 spectrometer at the Center for Chemical Characterization and Analysis (CCCA), Department of Chemistry, Texas A&M University. FT-IR data were collected by use of an IRAffinity-1 instrument. To obtain the TGA data, a TGA-50 (Shimadzu) thermogravimetric analyzer was used with a heating rate of $5\text{ }^\circ\text{C min}^{-1}$ under N_2 flow. The PXRD patterns were recorded by a Bruker D8-Focus Bragg–Brentano X-ray powder diffractometer equipped with a Cu sealed tube ($\lambda = 1.54178\text{ \AA}$) at a scan rate of 0.5 s deg^{-1} . All gas adsorption measurements were performed by Micromeritics' ASAP 2020 instrument with extra-purity gases. Based on the adsorption branch of N_2 adsorption isotherms of $R(N)$ -PCN-125, the pore size distributions were calculated by using DFT or Kruk–Jaroniec–Sayari (KJS) method in the Barrett–Joyner–Halenda (BJH) algorithm,²² provided in the ASAP 2020 software.

Synthesis and Characterization. The protonated ligands 1,1':4',1''-terphenyl-3,3'',5,5''-tetracarboxylic acid (H_4TPTC)¹³ and 5-aminomethylisophthalic acid²³ was synthesized according to the literature methods with slight modifications. All R -isoph (except 5-aminomethylisophthalic acid) and all starting materials were commercially available and used as received without further purification. Detailed descriptions of all syntheses and characterizations are given in the Supporting Information.

Synthesis of 5-(Aminomethyl)isophthalic Acid (NH_2CH_2 -isoph). To a solution of dimethyl 5-(azidomethyl)isophthalate²³ (0.52 g, 2.1 mmol) in THF (10 mL) were added water (2 mL) and triphenylphosphine (0.61 g, 2.3 mmol), and the resulting clear solution was stirred at room temperature for 12 h. Sodium hydroxide (1.0 N,

8.0 mL, 8.0 mmol) was then added, and the mixture was further stirred at room temperature for 8 h. The mixture was diluted in water (10 mL) and extracted with dichloromethane (40 mL) and then ethyl acetate (40 mL) to leave a slightly milky solution, which was acidified with hydrochloric acid (1.0 N, ~10 mL) to give a clear solution (pH ~5). THF (40 mL) was then added, and the solution was frozen at -20 °C overnight. Filtration, washing with ethanol, and drying under high vacuum afforded the desired product (0.36 g, 60% yield for two steps) as a white solid. ¹H NMR (with NaOH in D₂O, 300 MHz) δ 8.13 (t, 1 H, J = 1.7 Hz), 7.86(d, 2 H, J = 1.5 Hz), 3.81 (s, 2 H); ¹³C NMR (D₂O, 75 MHz) δ 175.8, 143.1, 137.3, 130.9, 128.2, 67.2 (p-dioxane, internal standard), 45.2.

Synthesis of R(N)-PCN-125. A mixture of H₄TPTC (40 mg, 0.1 mmol), R-isoph (0.1 or 0.2 mmol, amounts indicated in Table S1), and Cu(NO₃)₂·3H₂O (120 mg, 0.5 mmol) in 15 mL of N,N-dimethylacetamide (DMA) was sealed in a glass vial. The vial was tightly capped and placed in an 85 °C oven for 48 h to yield blue or green crystalline powders. For further analysis such as gas adsorption, PXRD, and NMR measurements, the crystalline powder samples were washed with fresh DMA (20 mL) and then immersed in fresh DMA (20 mL) for 1 day. Thorough washing with DMA is necessary to remove unreacted ligands in the crystals, and the NMR peaks of the ligands after digesting R(N)-PCN-125 become solely from the crystal and not from the surface-adsorbed one. Phase purity of all products was evaluated by PXRD. General characterizations including IR and TGA were carried out and are reported in the Supporting Information.

Gas Adsorption. Gas adsorption measurements were performed using an ASAP 2020 volumetric adsorption analyzer. A high-purity grade of gases was used throughout the adsorption experiments. Before adsorption, the sample was immersed in dry methanol for 72 h to remove the nonvolatile solvates. After the methanol was drained, chloroform was subsequently added, and the sample was allowed to sit for 72 h. After the removal of chloroform, the sample was dried under a dynamic vacuum (<0.1 mmHg) at room temperature overnight and then activated again at 100 °C by using the degassing port in ASAP 2020.

■ ASSOCIATED CONTENT

■ Supporting Information

Full syntheses of H₄TPTC and R(N)-PCN-125. PXRD and NMR data for control experiments to confirm the incorporation of R-isoph into the frameworks. PXRD and NMR data for multifunctionalized R(N)-PCN-125. N₂ and CO₂ adsorption isotherms, heats of CO₂ adsorption, FT-IR spectrum, and TGA data for all R(N)-PCN-125 prepared in this report. Pore size distribution calculated with N₂ adsorption isotherms at 77 K based on two different methods, DFT and KJS. Table summarizing the cell and refinement parameters from the PXRD. Table of BET and Langmuir surface areas, single-point total pore volumes, and DFT-based total pore volumes of R(N)-PCN-125. This material is available free of charge via the Internet at <http://pubs.acs.org>.

■ AUTHOR INFORMATION

Corresponding Author

zhouh@tamu.edu

Notes

The authors declare no competing financial interest.

■ ACKNOWLEDGMENTS

This work was supported by the U.S. Department of Energy (DOE DE-SC0001015, DE-AR0000073, and DE-FC36-07GO17033), the National Science Foundation (NSF CBET-0930079), and the Welch Foundation (A-1725).

■ REFERENCES

- (1) (a) Zhou, H.-C.; Long, J. R.; Yaghi, O. M. *Chem. Rev.* **2012**, *112*, 673. (b) Zhao, D.; Timmons, D. J.; Yuan, D.; Zhou, H.-C. *Acc. Chem. Res.* **2010**, *44*, 123. (c) Kitagawa, S.; Kitaura, R.; Noro, S. *Angew. Chem., Int. Ed.* **2004**, *43*, 2334. (d) O'Keeffe, M.; Yaghi, O. M. *Chem. Rev.* **2011**, *112*, 675.
- (2) (a) Li, J.-R.; Sculley, J.; Zhou, H.-C. *Chem. Rev.* **2012**, *112*, 869. (b) Li, J.-R.; Kuppler, R. J.; Zhou, H.-C. *Chem. Soc. Rev.* **2009**, *38*, 1477.
- (3) (a) Suh, M. P.; Park, H. J.; Prasad, T. K.; Lim, D.-W. *Chem. Rev.* **2012**, *112*, 782. (b) Sumida, K.; Rogow, D. L.; Mason, J. A.; McDonald, T. M.; Bloch, E. D.; Herm, Z. R.; Bae, T.-H.; Long, J. R. *Chem. Rev.* **2012**, *112*, 724. (c) Getman, R. B.; Bae, Y.-S.; Wilmer, C. E.; Snurr, R. Q. *Chem. Rev.* **2012**, *112*, 703.
- (4) (a) Kreno, L. E.; Leong, K.; Farha, O. K.; Allendorf, M.; Van Duyne, R. P.; Hupp, J. T. *Chem. Rev.* **2012**, *112*, 1105. (b) Rocha, J.; Carlos, L. D.; Paz, F. A. A.; Ananias, D. *Chem. Soc. Rev.* **2011**, *40*, 926.
- (5) Horcajada, P.; Gref, R.; Baati, T.; Allan, P. K.; Maurin, G.; Couvreur, P.; Férey, G.; Morris, R. E.; Serre, C. *Chem. Rev.* **2012**, *112*, 1232.
- (6) (a) Corma, A.; Garcia, H.; Xamena, F. X. L. *Chem. Rev.* **2010**, *110*, 4606. (b) Yoon, M.; Srirambalaji, R.; Kim, K. *Chem. Rev.* **2011**, *112*, 1196. (c) Ma, L.; Falkowski, J. M.; Abney, C.; Lin, W. *Nat. Chem.* **2010**, *2*, 838. (d) Yoon, M.; Srirambalaji, R.; Kim, K. *Chem. Rev.* **2012**, *112*, 1196.
- (7) (a) Almeida Paz, F. A.; Klinowski, J.; Vilela, S. M. F.; Tome, J. P. C.; Cavaleiro, J. A. S.; Rocha, J. *Chem. Soc. Rev.* **2012**, *41*, 1088. (b) Deng, H.; Doonan, C. J.; Furukawa, H.; Ferreira, R. B.; Towne, J.; Knobler, C. B.; Wang, B.; Yaghi, O. M. *Science* **2010**, *327*, 846. (c) Tanabe, K. K.; Cohen, S. M. *Chem. Soc. Rev.* **2011**, *40*, 498. (d) Cohen, S. M. *Chem. Rev.* **2012**, *112*, 970.
- (8) (a) Koh, K.; Wong-Foy, A. G.; Matzger, A. J. *Chem. Commun.* **2009**, 6162. (b) Park, T.-H.; Koh, K.; Wong-Foy, A. G.; Matzger, A. J. *Cryst. Growth Des.* **2011**, *11*, 2059.
- (9) (a) Koh, K.; Wong-Foy, A. G.; Matzger, A. J. *J. Am. Chem. Soc.* **2009**, *131*, 4184. (b) Koh, K.; Wong-Foy, A. G.; Matzger, A. J. *J. Am. Chem. Soc.* **2010**, *132*, 15005.
- (10) (a) Xuan, W.; Zhu, C.; Liu, Y.; Cui, Y. *Chem. Soc. Rev.* **2012**, *41*, 1677. (b) Yuan, D.; Zhao, D.; Timmons, D. J.; Zhou, H.-C. *Chem. Sci.* **2011**, *2*, 103. (c) Sun, L.-B.; Li, J.-R.; Park, J.; Zhou, H.-C. *J. Am. Chem. Soc.* **2011**, *134*, 126.
- (11) (a) Reboul, J.; Furukawa, S.; Horike, N.; Tsotsalas, M.; Hirai, K.; Uehara, H.; Kondo, M.; Louvain, N.; Sakata, O.; Kitagawa, S. *Nat. Mater.* **2012**, *11*, 717. (b) Mitchell, S.; Michels, N.-L.; Kunze, K.; Pérez-Ramírez, J. *Nat. Chem.* **2012**, *4*, 825.
- (12) (a) Wang, C. A.; Zhang, Z. K.; Yue, T.; Sun, Y. L.; Wang, L.; Wang, W. D.; Zhang, Y.; Liu, C.; Wang, W. *Chem. Eur. J.* **2012**, *18*, 6718. (b) Bunck, D. N.; Dichtel, W. R. *Angew. Chem., Int. Ed.* **2012**, *51*, 1885.
- (13) Lin, X.; Telepeni, I.; Blake, A. J.; Dailly, A.; Brown, C. M.; Simmons, J. M.; Zoppi, M.; Walker, G. S.; Thomas, K. M.; Mays, T. J.; Hubberstey, P.; Champness, N. R.; Schröder, M. *J. Am. Chem. Soc.* **2009**, *131*, 2159.
- (14) (a) Diring, S. P.; Furukawa, S.; Takashima, Y.; Tsuruoka, T.; Kitagawa, S. *Chem. Mater.* **2010**, *22*, 4531. (b) Tsuruoka, T.; Furukawa, S.; Takashima, Y.; Yoshida, K.; Isoda, S.; Kitagawa, S. *Angew. Chem., Int. Ed.* **2009**, *48*, 4739.
- (15) Fukushima, T.; Horike, S.; Kobayashi, H.; Tsujimoto, M.; Isoda, S.; Foo, M. L.; Kubota, Y.; Takata, M.; Kitagawa, S. *J. Am. Chem. Soc.* **2012**, *134*, 13341.
- (16) (a) Park, T.-H.; Hickman, A. J.; Koh, K.; Martin, S.; Wong-Foy, A. G.; Sanford, M. S.; Matzger, A. J. *J. Am. Chem. Soc.* **2011**, *133*, 20138. (b) Choi, K. M.; Jeon, H. J.; Kang, J. K.; Yaghi, O. M. *J. Am. Chem. Soc.* **2011**, *133*, 11920.
- (17) (a) Venna, S. R.; Jasinski, J. B.; Carreon, M. A. *J. Am. Chem. Soc.* **2010**, *132*, 18030. (b) Radha, A. V.; Kamath, P. V.; Shivakumara, C. *Acta Crystallogr., Sect. B* **2007**, *63*, 243.
- (18) (a) McDonald, T. M.; D'Alessandro, D. M.; Krishna, R.; Long, J. R. *Chem. Sci.* **2011**, *2*, 2022. (b) McDonald, T. M.; Lee, W. R.; Mason,

J. A.; Wiers, B. M.; Hong, C. S.; Long, J. R. *J. Am. Chem. Soc.* **2012**, *134*, 7056.

(19) Czepirski, L.; Jagiello, J. *Chem. Eng. Sci.* **1989**, *44*, 797.

(20) (a) Li, B.; Zhang, Y.; Ma, D.; Li, L.; Li, G.; Li, G.; Shi, Z.; Feng, S. *Chem. Commun.* **2012**, *48*, 6151. (b) Shiju, N. R.; Alberts, A. H.; Khalid, S.; Brown, D. R.; Rothenberg, G. *Angew. Chem., Int. Ed.* **2011**, *50*, 9615.

(21) (a) Im, S. G.; Bong, K. W.; Kim, B.-S.; Baxamusa, S. H.; Hammond, P. T.; Doyle, P. S.; Gleason, K. K. *J. Am. Chem. Soc.* **2008**, *130*, 14424. (b) Wendeln, C.; Rinnen, S.; Schulz, C.; Kaufmann, T.; Arlinghaus, H. F.; Ravoo, B. J. *Chem. Eur. J.* **2012**, *18*, 5880.

(22) (a) Choma, J.; Jaroniec, M.; Burakiewicz-Mortka, W.; Kloske, M. *Appl. Surf. Sci.* **2002**, *196*, 216. (b) Jaroniec, M.; Solovyov, L. A. *Langmuir* **2006**, *22*, 6757.

(23) Dimick, S. M.; Powell, S. C.; McMahon, S. A.; Moothoo, D. N.; Naismith, J. H.; Toone, E. J. *J. Am. Chem. Soc.* **1999**, *121*, 10286.